The submitted manuscript has been authored by a contractor of the U.S. Government under Contract No. DE-AC05-96OR22464. Accordingly, the U.S. Government retains a nonexclusive royalty-free license to publish or reproduce the published form of this contribution, or allow others to do so, for U.S. Government purposes.

Quasicoherent Fluctuations Associated with a Transport Barrier in the Sandpile Model*

H. R. Hicks and B. A. Carreras
Oak Ridge National Laboratory, Oak Ridge, TN 37830

Abstract

A transport barrier is introduced in the one-dimensional sandpile model by reducing the local flux in a barrier region. This reduction causes a modification in the structure of the avalanches and triggers quasiperiodic fluctuations of the particle fluxes. The frequency of these fluctuations is inversely proportional to the transport barrier width.

* Research sponsored by the Office of Fusion Energy, U.S. Department of Energy, under contract DE-AC05-00OR22725 with UT-Battelle, LLC.

I. INTRODUCTION

Models based on self-organized criticality (SOC)[1] have been developed to interpret some of the features of plasma transport in magnetically confined systems.[2,3] These models have been useful in showing the existence of some generic transport properties that subsequently have been confirmed in three-dimensional (3-D) turbulence calculations.[4,5,6] These models have also inspired experimental tests of plasma transport mechanisms.[7,8]

In the same spirit, here we use one of the simple SOC transport models to investigate some general properties of transport barriers.[9,10] Elsewhere,[11] a transport barrier mechanism based on sheared wind, coupled to a two-dimensional (2-D) sandpile, has been studied. The effect of the sheared wind is to produce a decorrelation of the avalanche in the barrier region.

Here, we consider a one-dimensional (1-D) sandpile and introduce the transport barrier as a simple modification of the sandpile rules. We change the sandpile rules by making the local instantaneous flux of particles a function of the radial position. Apart from the transport reduction induced by the barrier, this change causes a modification in the structure of the avalanches. Because of that, a quasiperiodic fluctuation is induced in the particle fluxes. The frequency of the fluctuations is inversely proportional to the transport barrier width.

To study the effect of a transport barrier in a sandpile is part of a broader issue of exploring the effect of inhomogeneities in an SOC system. These effects may be very important in man-made systems that operate close to a critical point.[12]

The rest of the article is organized as follows. In Sec. II, we explain the basic sandpile rules and introduce the transport barrier. The numerical results of the sandpile model with a transport barrier are described in Sec. III. In Sec. IV, we discuss changes to avalanche structure and the induced quasiperiodic behavior of fluxes. Finally, the conclusions of this study are set forth in Sec. V.

II. SANDPILE MODEL WITH TRANSPORT BARRIERS

The running sandpile model has been suggested as a paradigm for SOC turbulent plasma transport in magnetic confinement devices.[2,3] The sandpile model represents instability gradients by the slope of the sandpile, while the turbulent transport is modeled by the local amount of sand that falls (overturns) when the sandpile becomes locally unstable. In this model, a random rain of sand grains drives the system. This model enables us to

study the dynamics of the transport independent of the underlying instability mechanism that drives the turbulence.

We use a standard cellular automata algorithm[13] to study the dynamics of the driven sandpile. The domain is divided into L cells, which are evolved in steps. The number of sand grains in a cell is h_n, called the height of cell n. We take as radial position the value n that identifies the cell. The local gradient is Z_n, the difference between h_n and h_{n+1}, and Z_{crit} is the critical gradient. The standard sandpile evolution is governed by the following simple set of rules:

1) First, sand grains are added to the cells with a probability p_0. For each cell, a random number $0 \le p \le 1$ is drawn. If $p \ge 1 - p_0$, then

$$h_n = h_n + 1 \; ; \tag{1}$$

otherwise, the height h_n is not changed. This rule is used in studying transport dynamics. When we study the properties of individual avalanches, such as the size and duration of the avalanche, it is necessary to go to the limit of completely separated avalanches. That is the case when $p_0 \to 0$. To approach such a limit without an onerous expense of time, we change this rule. The new rule consists of dropping a grain of sand in a randomly selected cell. We then determine if an avalanche started. In the case of a negative answer, repeat the operation. Once an avalanche has started, no more sand is dropped while an avalanche is in progress. Naturally, this second version of rule (1) cannot be used in evaluating the transport dynamics, it only makes sense for evaluation of structural properties (size, duration, and space-time geometry) of individual avalanches.

2) Next, all the cells are checked for stability against a simple stability rule and either flagged as stable, $Z_n < Z_{crit}$, or not, $Z_n \ge Z_{crit}$.

3) Finally, the cells are time advanced, with the unstable cells overturning and moving their excess "grains" to another cell. That is, if $Z_n \ge Z_{crit}$, then

$$\begin{cases} h_n = h_n - N_f \\ h_{n+1} = h_{n+1} + N_f \end{cases} . \tag{2}$$

N_f is the amount of sand that falls in an overturning event, that is, the maximum local flux. In terms of the physical quantities that we associate with turbulent systems, each cell can be thought of as the location of a local turbulent fluctuation (eddy). Z_{crit} is the critical gradient at which fluctuations are unstable and grow, and N_f is the amount of "gradient" that is

transported by a local fluctuation (e.g., local eddy-induced transport). In this way, we can interpret the average sandpile profile as equivalent to the mean plasma temperature or density profile, while the total number of sand grains in the pile (the total mass) is the total energy/particle content of the device. At any given time, the local flux at a radial position is either zero, if this position is stable, or N_f, if it is unstable.

In a 1-D sandpile, a transport barrier can be implemented by increasing Z_{crit} in the barrier region by a factor F_{b} and at the same time decreasing N_{f} by the same factor. We introduce the parameter $N_{fb} = N_f / F_b$, which is the number of sand grains that are moved during an overturning event in the barrier region. If $F_{\mathrm{b}} \neq 1$, the homogeneity of the radial transport is broken. Note that a true transport barrier requires $F_{\mathrm{b}} > 1$. However, in studying the dynamical properties of this system, it is also interesting to consider the case $F_{\mathrm{b}} < 1$, an antibarrier.

We cannot expect that the change in the value of Z_{crit} will affect the dynamics of the sandpile because it has been shown[14] that the probability distribution of avalanche sizes is independent of the value of Z_{crit}. However, the local change of N_{f} can change the sandpile dynamics. We explore those changes in the next section.

III. NUMERICAL RESULTS FROM A SANDPILE MODEL WITH A TRANSPORT BARRIER

Numerical calculations have been carried out for a sandpile of size $L = 200$. We have located the center of the barrier at the cell $n = 100$, in the middle of the sandpile. Most of the results that we discuss in this article are not sensitive to the barrier location. We have chosen $Z_{\mathrm{crit}} = 100$ and $N_{\mathrm{f}} = 20$ for most of the calculations presented. With this value for N_{f}, we are able to consider a broad range of confinement improvement factors, F_{b}, while still keeping the N_{fb} integer. Unless otherwise stated, the barrier width is taken to be $W_{\mathrm{b}} = 20$.

Three measures are generally used to characterize an individual avalanche: (1) the avalanche size, S, the number of overturn events during the avalanche; (2) the avalanche duration, T, the number of time iterations during the avalanches; and (3) the flux out of the pile, Γ, induced by the avalanche. We use these three measures to study the statistical properties of the avalanches and how they have been modified by the presence of a transport barrier.

The sandpile dynamics is affected differently by changing the improvement factor, F_{b}. One way to observe this is by noting the number of avalanches directly affected by the existence of a barrier. A measure of this is the noninteger value of n_{w}. For the standard (barrier-less) sandpile, all avalanches are parallelograms (or lines) in space-time unless they

are truncated by the bottom edge of the sandpile and generate flux out of the system. For the standard sandpile one can prove that

$$n_w = \frac{1}{2}\left[T + 1 - \sqrt{(T+1)^2 - 4S - 2\frac{\Gamma}{N_f}\left(\frac{\Gamma}{N_f} - 1\right)}\right] \tag{3}$$

is an integer. In fact, n_w is the length of one side of the parallelogram. When a barrier is present, avalanches that intersect a barrier edge may take a more complex shape, indicating that the barrier has effected the avalanche. Such avalanches are seen to have a non-integer value of n_w. In Fig. 1, we have plotted the fraction of avalanches with the non-integer value of n_w as a function of N_{fb}. For $N_{fb} = 20$, the no-barrier case, this fraction is obviously zero. As N_{fb} decreases, this fraction goes through its maximum value for $N_{fb} = 10$. For $N_{fb} = 0$, the fraction of avalanches that is affected by the barrier goes to zero, because in this limit the transport barrier is impenetrable. Also, in Fig. 1, we have plotted the fraction of avalanches that overlaps with the transport barrier. For $N_{fb} < 10$, the latter practically coincides with the avalanches with non-integer n_w. However, as N_{fb} gets closer to N_f, the two fractions start to diverge as fewer and fewer of the avalanches crossing the barrier are affected by it.

The time-average slope of the sandpile, Z, depends on the value of the maximum local flux N_f;[15] that is, $\langle Z \rangle \approx Z_{crit} - N_f/2$. Because N_{fb} within the barrier is less than N_f outside the barrier, the sandpile slope in the barrier region is closer to the critical slope than it is outside the barrier. Therefore, the probability of an avalanche starting within the region of the barrier is higher than outside. This is shown in Fig. 2. In the same figure, we can see that the reverse occurs with an "antibarrier", where N_{fb} is higher than N_f outside the antibarrier.

In the way we have defined the transport barrier, the probability distribution functions (PDFs) of the avalanche sizes and of the flux out of the sandpile are not significantly affected by the barrier. What is affected is the duration of the avalanches crossing the barrier. In Fig. 3, we have plotted the PDFs of the avalanche sizes for different values of N_{fb}. We can see that the PDFs are effectively the same for all values of N_{fb}. We can also consider the integrated fluxes out of the sandpile associated with each avalanche. The PDF of the integrated fluxes is also unchanged by the presence of a transport barrier (Fig. 4). However, the transport barrier does slow down transport through that region. This effect can be seen in Fig. 5 by the change in the PDF of the duration of the avalanches. Naturally, the change in duration affects only the avalanches that cross the barrier, but the largest avalanches are in this set. The largest avalanches are

the most important ones for the overall sandpile confinement. The PDF shows a larger tail of avalanche duration when there is a barrier.

The PDF of the avalanche duration is also affected by the barrier width, W_b. All previous results where obtained for a barrier width of 20. In Fig. 6, we show the PDFs of the avalanche duration for different values of W_b. For a sandpile without a barrier, the maximum avalanche duration is equal to the length of the sandpile. For the case plotted in Fig. 6 this value is 200 and it is the cut-off value of the PDF for $W_b = 0$. We can see that as W_b increases, the PDF tail reaches to larger values of duration (e.g., for durations 3000). However, the probability of these events decreases for large values of W_b (for example, the $W_b = 80$ case for durations from 300 to 2000) because the avalanches that are lengthened as a result of the barrier are the avalanches that go across the whole barrier width. As the barrier widens, its effect becomes more important; but there are fewer avalanches that can go all the way across.

IV. AVALANCHE STRUCTURE AND QUASIPERIODIC FLUCTUATIONS

One of the more interesting effects of a transport barrier is the change of the structure of the avalanches that cross the transport barrier (Fig. 7). When an avalanche that starts above the barrier reaches the barrier, it produces an accumulation of particles at the boundary. Because the amount of flux that can be transported across is reduced, the accumulated particles must be taken across the barrier through multiple internal mini-avalanches, which in succession trigger avalanches at the lower edge of the barrier. By looking at the radius vs time plots of the unstable sites, we can visualize the space-time structure of the avalanches. For the standard sandpile, this structure is either 1-D (a line) or 2-D (a parallelogram). This is the case in Fig. 7 of the avalanches that do not cross the barrier. This is the geometrical structure that leads to n_w being an integer. However, for the avalanches that cross the barrier, the space-time structure is much more complicated. As described previously, the subavalanches in the barrier travel across this region as many times as needed to transport all of the grains that were deposited at the top by the initiating avalanche. The initiating avalanche can also be below the transport barrier region because of the double propagation of the 2-D avalanches. In this case, it is a deep hole at the lower edge of the barrier that triggers a sequence of avalanches across the barrier in a similar manner. Because of these mechanisms, there is a basic period associated with this process, twice the barrier width times the velocity of the avalanche. Therefore, the corresponding frequency of avalanches emerging from the barrier is

$$f = \frac{w_k}{2W_b}\frac{1}{\tau_k} \ , \tag{4}$$

where w_k is the unit of length and τ_k is the unit of time. Making the correspondence to plasma transport, w_k is the turbulent eddy width, and τ_k is the eddy turnover time.

The space-time structure of the avalanches translates into a quasiperiodic behavior of the fluxes emerging from the barrier. The power spectrum of the flux at the outer edge of the transport barrier is characterized by the power spectrum shown in Fig. 8. The figure indicates the clear presence of peaks in the spectrum. We have cut the very high frequency end of the spectrum because it only reflects the discrete nature of the time sequence of flux. In Fig. 8, we can expect the lowest frequency peak to be associated with the frequency given by Eq. (4). The other peaks are harmonics of this frequency. The integer character of the flux makes the presence of harmonics quite marked. In more realistic systems we expect an effective damping of the high harmonics. To show that the frequency peaks in the spectrum are linked to the frequency given by Eq. (4), we have plotted in Fig. 9 these frequency peaks times the barrier width for several values of the barrier width. The plot shows that Eq. (4) reproduces the main harmonic for all cases considered.

The numerical results also show a very weak dependence of the main frequency on the value of N_{fb}, for $N_{fb} < N_f$. This dependence is not given by Eq. (4); it only changes the frequency by about 10%. There is a dramatic change for $N_{fb} > N_f$. In this case, the barrier changes to antibarrier, and there is an acceleration of the fluxes across this region. Therefore, the accumulation of particles at the top of the barrier no longer occurs and so there are no quasiperiodic fluctuations.

V. CONCLUSIONS

We have introduced in a very simple manner a transport barrier in a sandpile model. In the way this model is constructed, the barrier causes an automatic increase of the sandpile gradient in the barrier region. There is a further dynamical effect on the avalanches. That is to increase the duration of the largest avalanches by slowing down transport across the barrier. This naturally improves the confinement of the particles.

The presence of such a barrier modifies the structure of the avalanches and introduces quasiperiodic behavior of the fluxes. The period of this quasiperiodic motion is inversely proportional to the barrier width.

This type of quasiperiodic oscillation may be related to some observations of quasiperiodic fluctuations during the enhanced D_α H-mode[16] in the Alcator C-mod tokamak. These quasicoherent fluctuations have been determined with several diagnostics. One observation is that the frequency of these fluctuations is proportional to the inverse of the pedestal width.[17] If we identify the barrier region with the region of the pedestal, this observation is consistent with the previous results, and the observed fluctuations may be induced by the fluctuating fluxes.

ACKNOWLEDGMENTS

One of the authors (B. A. Carreras) would like to acknowledge fruitful discussions with Martin Greenwald. This research was sponsored by the Office of Fusion Energy, U.S. Department of Energy, under contract DE-AC05-00OR22725 with UT-Battelle, LLC.

REFERENCES

[1]P. Bak, C. Tang, and K. Wiesenfeld, Phys. Rev. Lett. **59,** 381 (1987).

[2]P. H. Diamond and T. S. Hahm, Phys. Plasmas **2,** 3640 (1995).

[3]D. E. Newman, B. A. Carreras, P. H. Diamond, and T. S. Hahm, Phys. Plasmas **3,** 1858 (1996).

[4]B. A. Carreras, D. Newman, V. E. Lynch, and P. H. Diamond, Phys. Plasmas **3,** 2903 (1996).

[5]X. Garbet and R. E. Waltz, Phys. Plasmas **5,** 2836 (1998).

[6]S. Benkadda, P. Beyer, X. Garbet, and Y. Sarazin, Phys. Scripta T**84**, 14 (2000).

[7]P. A. Politzer, Phys. Rev. Lett. **84**, 1192 (2000).

[8]B. A. Carreras, B. van Milligen, M. A. Pedrosa, R. Balbín, C. Hidalgo, D. E. Newman, E. Sánchez, M. Frances, I. Garcia-Cortes, J. Bleuel, M. Endler, S. Davies, and G. F. Matthews, Phys. Rev. Lett. **80** (20), 4438(1998).

[9]K. H. Burrell, Phys. Plasmas **4,** 1499 (1997).

[10]P. W. Terry, Rev. Modern Phys. **72**, 109 (2000).

[11]D. E. Newman, B. A. Carreras, and P. H. Diamond, Phys. Lett. A **218**, 58 (1996).

[12]B. Carreras, V. E. Lynch, M. L. Sachtjen, I. Dobson, and D. E. Newman, "Modeling Blackout Dynamics in Power Transmission Networks with Simple Structure"; Proceedings 34th Hawaii International Conference on System Sciences, Maui, Hawaii, January 2001.

[13]T. Hwa and M. Kadar, Phys. Rev. A **45,** 7002 (1992).

[14]L. P. Kadanoff, S. R. Nagel, L. Wu, and S.-M. Zhou, Phys. Rev. A **39,** 6524 (1989).

[15]M. V. Medvedev, P. H. Diamond, and B. A. Carreras, Phys. Plasmas **3** (10), 3745 (1996).

[16]M. Greenwald, R. Bovin, P. Bonoli, R. Budny, C. Fiore, J. Goetz, R. Granetz, A. Hubbard, I. Hutchinson, J. Irby, B. LaBombard, Y. Lin, B. Lipschultz, E. Marmar, A. Mazurenko, D. Mossessian, T. Sunn Pedersen, C. S. Pitcher, M. Porkolab, J. Rice, W. Rowan, J. Snipes, G. Shilling, Y. Takase, J. Terry, S. Wolf, J. Weaver, B. Welch, and S. Wukitch, Phys. Plasmas **6**, 1943 (1999).

[17]M. Greenwald, R. Bovin, P. Bonoli, C. Fiore, J. Goetz, R. Granetz, A. Hubbard, I. Hutchinson, J. Irby, Y. Lin, E. Marmar, A. Mazurenko, D. Mossessian, T. Sunn Pedersen, J. Rice, G. Shilling, G. Taylor, J. Terry, S. Wolf, and S. Wukitch, Plasma Phys. Control. Fusion **42**, A263 (2000).

FIGURE CAPTIONS

Fig. 1. With $N_f = 20$ outside the barrier, N_{fb} within the barrier is varied. The fraction of avalanches with noninteger n_w is identically zero for $N_{fb} = N_f$ and for $N_{fb} = 0$; while the fraction of the avalanches crossing either barrier edge is only zero for $N_{fb} = 0$.

Fig. 2. Probability of an avalanche starting at a given position comparing a case with no barrier ($N_{fb} = 20$) to a case with a barrier ($N_{fb} = 10$) and an antibarrier ($N_{fb} = 100$). The barrier corresponds to positions 90–110, and $N_f = 20$ in all three cases.

Fig. 3. The PDF of the avalanche size, *S*, measured by the total number of overturns in the avalanche, which is independent of N_{fb}.

Fig 4. The PDF of flux, Γ, out of the bottom of the avalanche, which is independent of N_{fb}.

Fig. 5. The PDF of the duration of avalanches (in time steps), *T*, showing a larger tail when a barrier is present. These calculations are for 10^7 time steps, and represent at least 1.4×10^5 avalanches. Each point plotted represents the average of at least 50 avalanches, and the maximum statistical error of any point plotted is 14%.

Fig. 6. The PDF of the duration of avalanches (in time steps), *T*, plotted for different values of the transport barrier width. These calculations are for 10^7 time steps, and represent at least 1.4×10^5 avalanches. Each point plotted represents the average of at least 50 avalanches, and the maximum statistical error of any point plotted is 14%.

Fig. 7. Space-time plot of avalanches with barrier present. The top of the sandpile is at radial position 0; the bottom is at radial position 200.

Fig. 8. Power spectrum of the flux at the outer edge of the transport barrier. The spectrum has clear peaks at the frequency given by Eq. (4) and its harmonics.

Fig. 9. Frequency peaks of the power spectrum of the flux times the barrier width for several values of the barrier width. The plot shows that Eq. (4) reproduces the main harmonic for all cases considered.

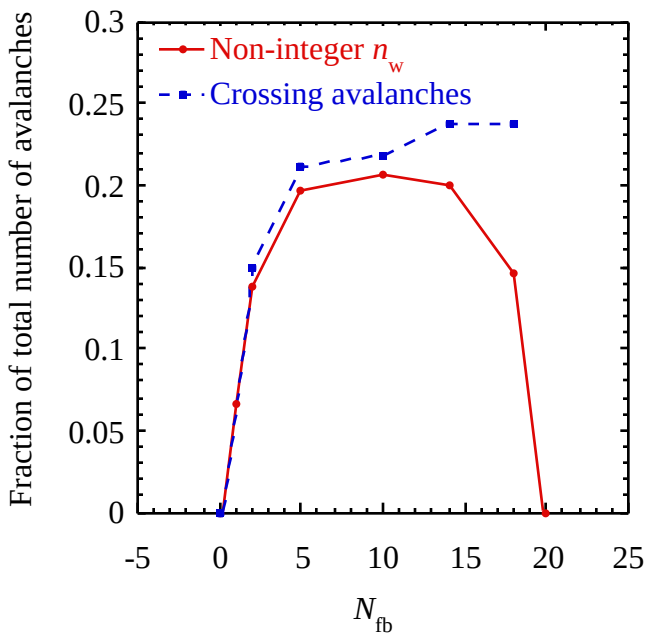
Non-integer n_w
Crossing avalanches
Fraction of total number of avalanches
0.3
0.25
0.2
0.15
0.1
0.05
0
-5
0
5
10
15
20
25
N_{fb}

Fig. 1

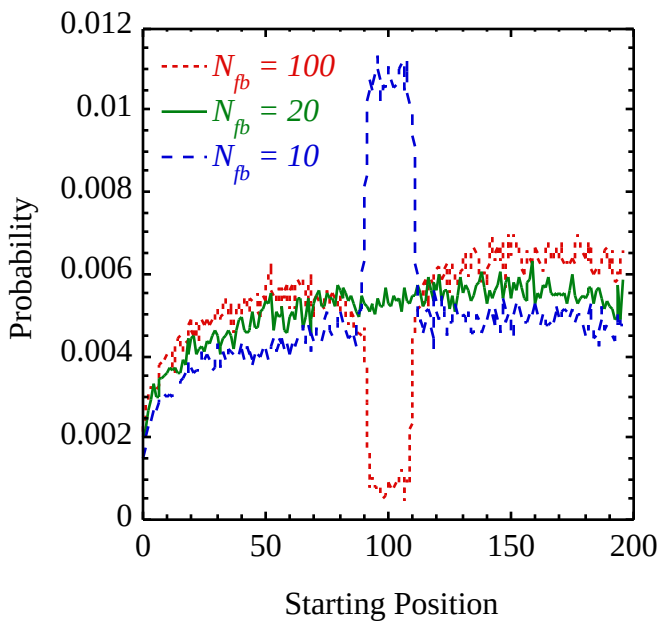
N_{fb} = 100
N_{fb} = 20
N_{fb} = 10
Probability
0.012
0.01
0.008
0.006
0.004
0.002
0
0
50
100
150
200
Starting Position

Fig. 2.

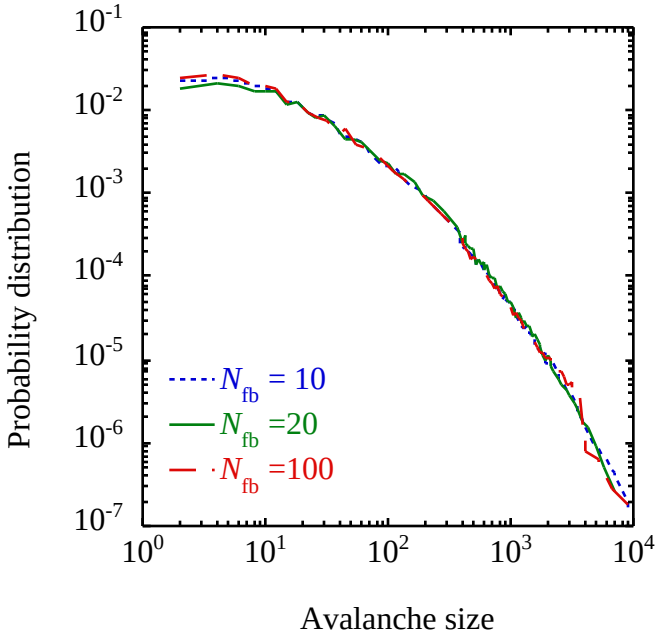
Probability distribution
Avalanche size
N_{fb} = 10
N_{fb} =20
N_{fb} =100

Fig 3

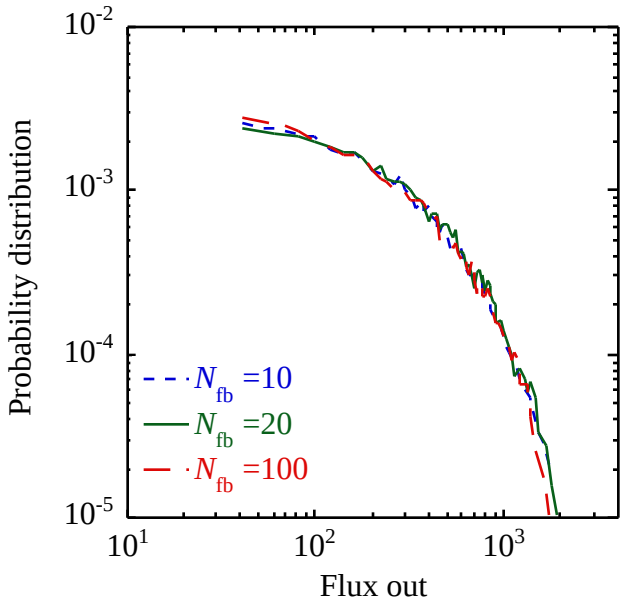
Probability distribution
Flux out
N_{fb} =10
N_{fb} =20
N_{fb} =100

Fig. 4

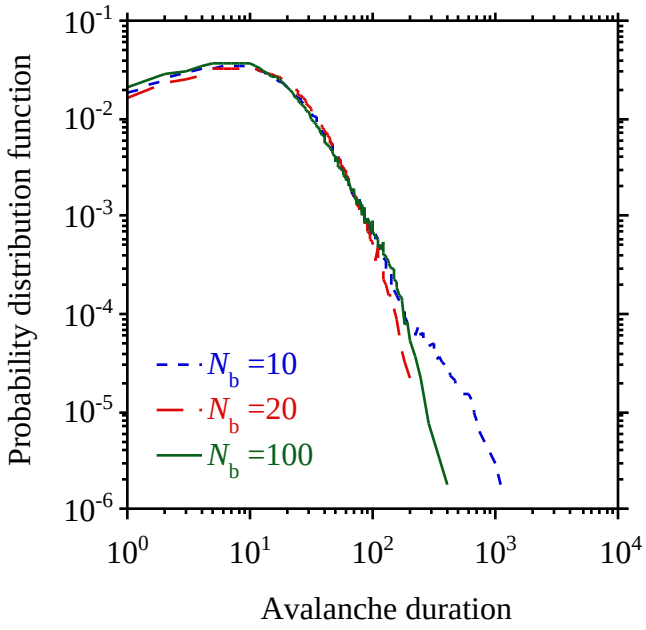
Probability distribution function
Avalanche duration
N_b =10
N_b =20
N_b =100

Fig. 5

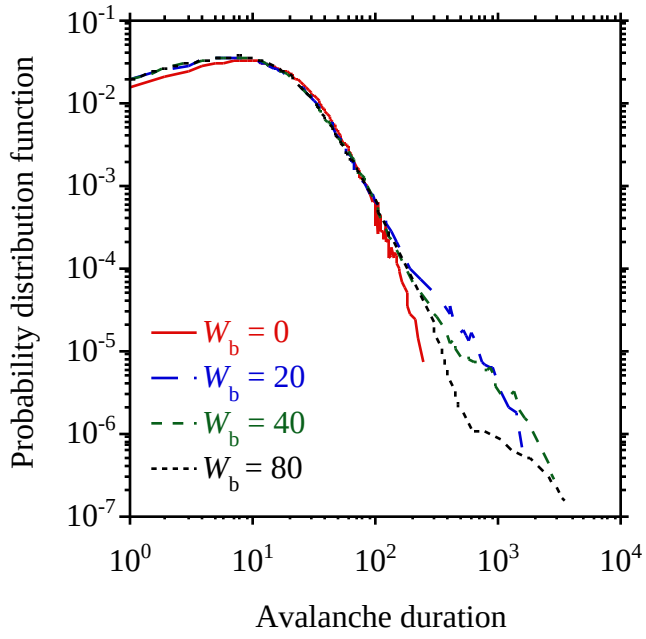
Probability distribution function
Avalanche duration
W_b = 0
W_b = 20
W_b = 40
W_b = 80

Fig. 6.

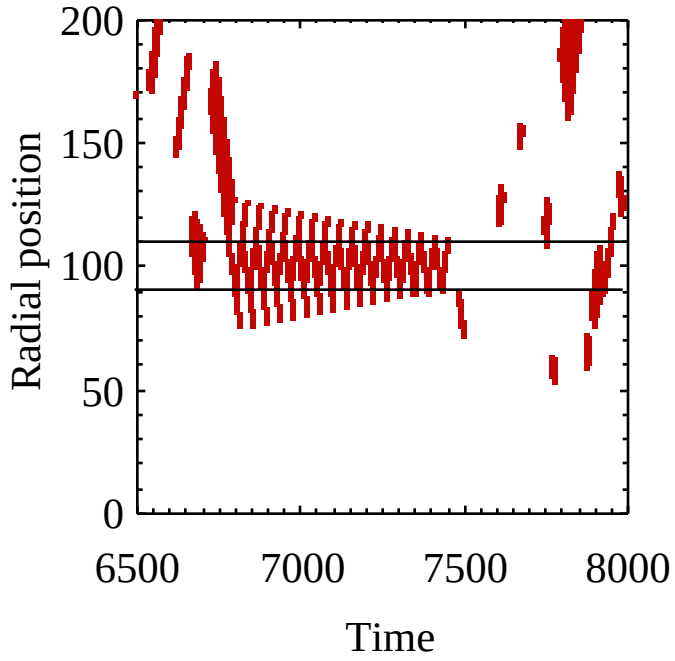
200
150
100
50
0
Radial position
6500
7000
7500
8000
Time

Fig. 7

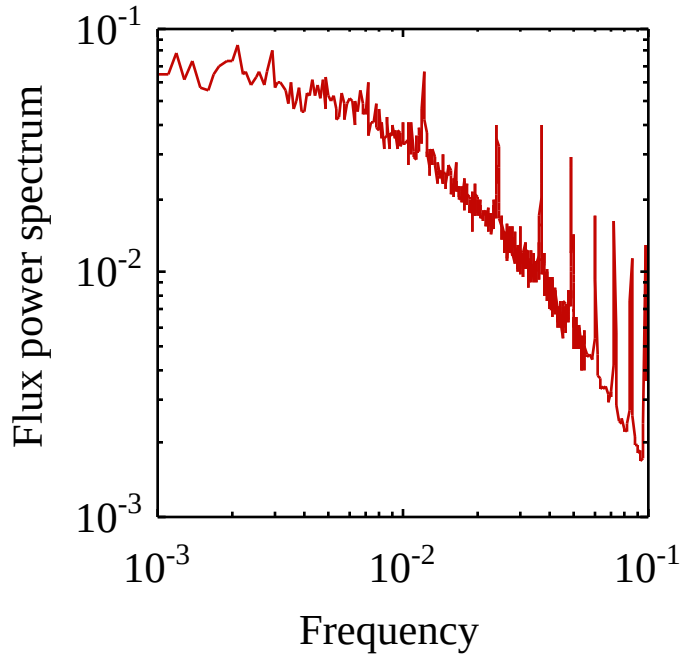
10-1
10-2
10-3
Flux power spectrum
10-3
10-2
10-1
Frequency

Fig. 8

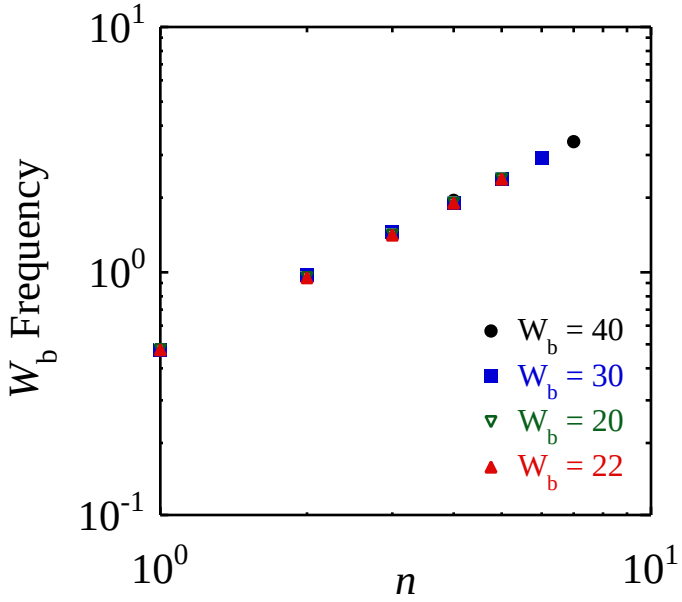

Fig. 9